Accepted manuscript:

Decoupled Hf and Nd isotopes in suspended particles and in the dissolved load of Late Archean seawater

by

Sebastian Viehmann[a,b],, Michael Bau[a], J. Elis Hoffmann[c], Carsten Münker[d]

[a] Jacobs University Bremen, Department of Physics and Earth Sciences, Campus Ring 1, 28759 Bremen, Germany
[b] Universität Wien, Department of Geodynamics and Sedimentology, Althanstr. 14, 1090 Wien, Austria
[c] Freie Universität Berlin, Department of Earth Sciences, Geochemistry, Malteserstr. 74-100, 12249 Berlin, Germany
[d] Universität zu Köln, Institut für Geologie und Mineralogie, Zülpicher Str. 49b, 50674 Köln, Germany

https://doi.org/10.1016/j.chemgeo.2018.01.017

Received 12 June 2017; Received in revised form 21 December 2017; Accepted 17 January 2018

Available online 31 January 2018(Embargo: 24 months)

Decoupled Hf and Nd isotopes in suspended particles and in the dissolved load of Late Archean seawater

Sebastian Viehmann[1,2*], Michael Bau[1], J. Elis Hoffmann[3], Carsten Münker[4]

[1] Jacobs University Bremen, Department of Physics and Earth Sciences, Campus Ring 1, 28759 Bremen, Germany

[2] Universität Wien, Department for Geodynamics and Sedimentology, Althanstr. 14, 1090 Wien, Austria

[3] Freie Universität Berlin, Department of Earth Sciences, Geochemistry, Malteserstr. 74-100, 12249 Berlin, Germany

[4] Universität zu Köln, Institut für Geologie und Mineralogie, Zülpicher Str. 49b, 50674 Köln, Germany

*corresponding author: Sebastian Viehmann, sebastian.viehmann@univie.ac.at
Tel. +43 1 4277 53680
Universität Wien

First version, Chemical Geology

June, 2017

Abstract

It is generally agreed that decoupling of the Hf and Nd isotope systems in modern aqueous systems is a result of incongruent release of Hf during terrestrial weathering of the continental crust, although the mechanism(s) behind this process are not yet fully understood. We here present Hf-Nd isotope data for the Neoarchean Krivoy Rog Banded Iron Formation (BIFs), Ukraine, and combine observations on modern aqueous environments with those of the early Earth to further evaluate the mechanism(s) behind Hf-Nd isotope decoupling in aqueous systems.

The pure Late Archean Krivoy Rog chemical sediment endmember, representing the dissolved pool of ancient seawater, shows decoupled $\varepsilon Nd_{2.60Ga}$-$\varepsilon Hf_{2.60Ga}$ values of -2.3 and +9.48, respectively, and suggests that decoupled Hf-Nd isotopes had been a *global* rather than a *local* phenomenon in Neoarchean seawater. This further reveals that incongruent Hf release via terrestrial weathering and erosion of emerged and evolved continental landmasses were widespread geological processes by Late Archean time.

Impure Krivoy Rog BIF samples, composed of a mixture of seawater-derived and detrital Nd and Hf, show systematically more positive $\varepsilon Nd_{2.60Ga}$ values, but still reveal decoupled εNd-εHf values relative to an associated schist that plots slightly below the 'terrestrial array'. This suggests that mineral sorting between a zircon-bearing sand-sized fraction and fine-grained sediment particles occurred on/in Late Archean continents, rivers and oceans, and had significant impact on the chemical compositions of the suspended and dissolved element loads of Late Archean seawater. Less radiogenic Hf isotope compositions in the Krivoy Rog seawater relative to detritus-contaminated BIFs further suggest a pathway for high-temperature hydrothermal Hf into anoxic Archean seawater, that diluted the even more radiogenic Hf isotopic composition of continental run-off, created by the mineralogical composition of the continental hinterland and the 'zircon effect'. Alternatively, the less pronounced decoupling of εHf-εNd in Late Archean seawater may be related to a shorter

residence time of Hf relative to Nd. Furthermore, systematically more positive initial εNd values in detritus-contaminated Archean BIFs relative to respective dissolved seawater loads suggest that weathered and eroded material of (ultra)mafic rock suites had significant impact on the suspended and dissolved fractions in Archean seawater.

Keywords

Hf-Nd isotopes; Seawater; BIF; Zircon effect; Archean

1. Introduction

The Hf and Nd isotope systems are powerful proxies in high-temperature geochemistry to gather precise information about metamorphic and depositional ages of (meta-) igneous rock series, but also to unravel magma differentiation, fractional crystallization and mixing processes occurring in early Earth mantle and crust (e.g. Hoffmann et al., 2011; Szilas et al., 2015; Hoffmann et al., 2016; Szilas et al., 2016). While both isotope systems are coupled in magmatic regimes (e.g. Vervoort et al., 1999), their behavior in low-temperature environments such as natural waters is more complicated and the two isotope systems behave differently (e.g. Patchett et al., 1984; Albarede et al., 1998; van de Flierdt et al., 2004; Rickli et al., 2009; Stichel et al., 2012; Viehmann et al., 2014).

The residence time of particle-reactive elements such as rare earth elements (REE) and Hf in modern oxidized oceans is shorter than the mixing time needed to homogenize global seawater (Piepgras and Wasserburg, 1980; Tachikawa et al., 1999; Rickli et al., 2009). Piepgras and Wasserburg (1980) and subsequent research applied Nd isotopes as reliable tracers to determine the source of REE and to track movement of water masses of modern (e.g. Piepgras and Wasserburg, 1980) and ancient seawater (e.g. Miller and O´Nions, 1985; Alibert and McCulloch, 1993; Alexander et al., 2009; Viehmann et al., 2015a; 2015b; Viehmann et al., 2016). It appears that Nd is weathered congruently from the continents and that the Nd

79 isotopic composition of modern seawater resembles the Nd isotopic composition of the
80 terrigenous hinterland (for a recent compilation of Nd isotopes in modern seawater see van de
81 Flierdt et al., 2016 and Tachikawa et al., 2017). High-temperature hydrothermal vent sites
82 with their abundant black smokers are sinks rather than sources for REE in modern oxidized
83 oceans and, therefore, their REE contribution to the global seawater REE budget is rather
84 negligible (German et al., 1990). In contrast, there is strong evidence that high-temperature
85 hydrothermal fluids expelled Fe and other elements into the *anoxic* Archean seawater which
86 was the reservoir from which early Precambrian banded iron-formations (BIFs) precipitated
87 (e.g. Fryer et al., 1979; Danielson et al., 1992; Bau and Dulski, 1996; Bau and Alexander,
88 2009; Alexander et al., 2009; Bekker et al., 2010; Li et al., 2015; Viehmann et al., 2015a).
89 Due to analytical challenges, results of direct Hf isotope measurements of seawater
90 were first reported in 2009 (Godfrey et al., 2009; Rickli et al., 2009; Zimmermann et al.,
91 2009), but confirmed previous studies which used hydrogenetic Fe-Mn crusts as seawater
92 archives (e.g. Patchett et al., 1984; Albarede et al., 1998; van de Flierdt et al., 2004; van de
93 Flierdt et al., 2007). These studies reported a partial decoupling of the Hf and Nd isotope
94 systems in seawater, i.e. at given a εNd value, the corresponding εHf value is more positive in
95 seawater than it is in ambient terrestrial rocks. Patchett et al. (1984) introduced the term
96 'zircon effect' to describe incongruent Hf release during weathering of continental crust due to
97 retention of unradiogenic Hf in weathering-resistant zircons. Hence, the easily weathered and
98 eroded element and isotope fraction of the continental crust that is transferred to seawater via
99 rivers or atmospheric dust shows more positive εHf values than the weathered bulk rock,
100 resulting in more radiogenic εHf values of seawater (e.g. Patchett et al., 1984; Albarede et al.,
101 1998; Bayon et al., 2006; Rickli et al., 2009; Garcon et al., 2013; 2014; Bayon et al., 2016). In
102 detail, the slightly different residence times of Hf and Nd in modern seawater (Rickli et al.,
103 2014; Filippova et al., 2017) as well as the mineralogical composition of the weathered
104 hinterland (Bayon et al., 2006; Chen et al., 2013; Garcon et al., 2014b; Bayon et al., 2016,

105 Garcon et al., 2017; Rickli et al., 2017), mineral sorting during aeolian processes (e.g.
106 Albarede et al., 1998, Pettke et al., 2002; Chen et al., 2013) and in rivers (Garcon et al., 2013;
107 2014b), ambient weathering conditions in the continental hinterland (Rickli et al., 2013;
108 Bayon et al., 2016; Rickli et al., 2017), and the abundance of nanoparticles and colloids in
109 river water (Merschel et al., 2017b) are factors which control the decoupling of the Hf-Nd
110 isotope systems in modern rivers and oceans. The weathering of accessory minerals such as
111 phosphates, carbonates or garnets with high Lu/Hf ratios (Bayon et al., 2006; Rickli et al.;
112 2013; Garcon et al., 2014b; Rickli et al., 2017), the water-rock interaction time during
113 weathering (Rickli et al., 2017) and hydrodynamical mineral sorting between 'heavy' zircon-
114 bearing sand-sized fractions (i.e. bedload material) and smaller zircon-poor, fine-grained
115 fractions that remain in the suspended particle load (> 0.2 μm) of rivers with higher bulk εHf
116 values (Garcon et al., 2013; 2014b), respectively, already fractionate the Hf isotope
117 composition in rivers on the continents and finally increase the εHf value of the suspended
118 and "dissolved" fractions (< 0.2 μm) entering the estuarine system of modern oceans. A
119 similar relationship between εHf and εNd is also observed between ultra-filtered ("truly
120 dissolved") and 0.2 μm-filtered ("dissolved") river waters, suggesting that decoupling of Hf
121 and Nd isotopes between the truly dissolved and the dissolved (i.e. nanoparticulate) Hf and
122 Nd fraction in river water is also significant and that the difference between the truly
123 dissolved and the suspended particle fraction is even more pronounced than that between the
124 dissolved (i.e. nanoparticulate) and the suspended fraction (Merschel et al., 2017b).
125 Furthermore, Viehmann et al. (2014) observed decoupling of Hf-Nd isotopes in very pure
126 chemical sediments (cherts and BIFs) from the ~2.7 Ga old Temagami greenstone belt, which
127 represent the dissolved fraction of Late Archean Temagami seawater, and concluded that
128 incongruent weathering and erosion processes of zircon-bearing, emerged continental crust
129 were already operating in the Neoarchean. We here present high precision Hf and Nd isotope
130 data supported by trace element analyses of pure and detritus-contaminated BIF samples from

131 the Neoarchean Krivoy Rog BIF, Ukraine, to combine observations made in modern aqueous
132 environments with those on early Earth to further evaluate the mechanism(s) which cause the
133 decoupling of Hf and Nd isotopes in Late Archean seawater.
134
135 ## 2. Geological overview of the Neoarchean Krivoy Rog BIF
136 The greenschist- to amphibolite-facies Krivoy Rog Supergroup is located in the
137 western part of the Middle Dnieper granite-greenstone terrain of the Ukrainian Shield, Central
138 Ukraine. Clastic and chemical metasediments discordantly overlie Mesoarchean basement of
139 the Konka and Belozerka Supergroups and are described in more detail elsewhere (e.g. Kulik,
140 1991; Kulik and Korzhnev, 1997; Bibikova et al., 2010). The up to 1400 m thick BIF of the
141 Saxagan Group is defined as Superior-type BIF, i.e. Fe-rich and Si-rich banded chemical
142 sediments alternate with clastic sedimentary units that were deposited during cycles of
143 transgression and regression periods of the Krivoy Rog sea (Kulik et al., 1991). The
144 depositional age of the chemo-clastic Krivoy Rog Supergroup was bracketed between 2.7 and
145 2.0 Ga (Shcherbak et al., 1984; 1989). More recently, Viehmann et al. (2015a) favored a Late
146 Archean rather than a Proterozoic depositional age, because of the omnipresence of large
147 positive Eu anomalies in chondrite-normalized REE patterns of Krivoy Rog BIFs. While such
148 anomalies are common in Archean marine chemical sediments, they are extremely rare in
149 Proterozoic ones and may thus be used as qualitative dating tool.
150
151 ## 3. Analytical Methods
152 The homogenous sample powders of the Krivoy Rog BIF described in Viehmann et al.
153 (2015a) and the BIF standard IF-G were analyzed in two subsequent batches together with
154 BIF samples of Viehmann et al. (2014). Approximately 200 mg of BIF and 100 mg of schist
155 powder were spiked with mixed ^{180}Ta-^{180}Hf-^{176}Lu-^{94}Zr and a ^{149}Sm-^{150}Nd tracers and digested
156 in HF-HNO_3 mixture in Parr® bombs at 180°C for 75h. After subsequent dry down the

157 residues were immediately treated with $HCLO_4$ to ensure complete digestion, followed by
158 further dry down steps with conc. HNO_3 + trace HF and overnight sample-spike equilibration
159 in 6 N HCl + 0.06 HF at 120°C. The analytical procedures follow protocols that are described
160 in more detail elsewhere (Pin and Zalduegui, 1997; Münker et al., 2001; Weyer et al., 2002;
161 Alexander, 2008; Viehmann et al., 2014; Viehmann et al., 2015a).
162 After ion exchange separation of the isotope aliquots, the isotope compositions and the
163 concentrations of Lu, Hf and Sm, Nd were determined by isotope dilution technique and
164 Finnigan® Neptune MC-ICPMS analyses in the joint Cologne-Bonn facility at the University
165 of Bonn. Detailed information about mass bias correction methods, internal standards, the
166 reference standard IF-G, external reproducibility and blanks measured during the course of
167 study have already been published in Viehmann et al. (2014) and Viehmann et al. (2015a). In
168 short, Hf isotope data were mass bias corrected to a $^{179}Hf/^{177}Hf$ ratio of 0.7325 using the
169 exponential law, and are given here relative to the $^{176}Hf/^{177}Hf$ ratio of 0.282160 of the
170 Münster AMES standard with an external reproducibility of ±40 ppm (2σ), that is
171 indistinguishable from the JMC-475. The typical external reproducibility was ±0.2% (2σ) for
172 $^{176}Lu/^{175}Hf$.
173 For calculation of initial εHf and εNd values, the ^{176}Lu decay constant of $1.876 * 10^{-11}$
174 (Scherer et al., 2001; Söderlund et al., 2004), the ^{147}Sm decay constant of $6.54 * 10^{-11}$
175 (Lugmair and Marti, 1978) and the CHUR (CHondritic Uniform Reservoir) parameter of
176 Bouvier et al. (2008) were applied. Error bars of Lu-Hf isochron calculations were calculated
177 using the error propagation method based on uncertainties of minimum and maximum blank
178 concentrations.
179
180 ## 4. Results
181 The Lu-Hf and Sm-Nd isotope data of the Krivoy Rog BIF are listed in Table 1. Ratios
182 of $^{176}Lu/^{177}Hf$ range from 0.02007 in the Krivoy Rog schist to 0.23046 and 0.30650 in the

183 pure chemical sediment endmember of BIF samples (for a definition of the endmember, see
184 Viehmann et al., 2015a). Initial εHf values of the Late Archean Krivoy Rog BIF samples are
185 very heterogeneous and considerably more positive than their respective $\varepsilon Nd_{2.60Ga}$ values
186 which fall in the range between -2.3 ± 0.4 to +0 ± 0.4; the purest BIF sample which preserved
187 the isotope composition of seawater, shows the most negative $\varepsilon Nd_{2.60Ga}$ value (Viehmann et
188 al., 2015a, Table 1). The $\varepsilon Hf_{2.60Ga}$ values of pure and impure Krivoy Rog BIF samples range
189 from almost chondritic (-0.91 ± 1.2) to strongly positive (up to +60.6 ± 1.0; Table 1). A
190 combined Lu-Hf isochron of pure *and* impure Krivoy Rog BIF samples yields 2775 ±160 Ma
191 (Figure 1) and overlaps within error with the proposed Late Archean depositional age
192 (Viehmann et al., 2015a), indicating only very minor to negligible post-depositional
193 alterations or reset of the Hf isotope system during up-to-amphibolite facies metamorphic
194 events around 2.0 Ga (Shcherbak et al., 1984). However, the geochronological significance of
195 this Hf isochron has to be questioned due to the fact that the isochron is spanned between a
196 pure chemical sediment endmember with high $^{176}Lu/^{177}Hf$ and $^{176}Hf/^{177}Hf$ ratios and detritus-
197 contaminated samples with lower $^{176}Lu/^{177}Hf$ and $^{176}Hf/^{177}Hf$ ratios, respectively. In contrast
198 to coupled Sm-Nd and Lu-Hf isochrons of ultrapure BIF from the Late Archean Temagami
199 Greenstone Belt that overlap with the published depositional age and provide valuable
200 geochronological information (Viehmann et al., 2014), the Hf "isochron" of the Krivoy Rog
201 BIFs rather represents a mixing line between detrital and seawater Hf, which is further
202 supported by mixing calculations between the chemical sediment and the schist sample
203 (Figure 2). This observation is further strengthened by REY and HFSE relationships of the
204 same sample set, that were used to distinguish between pure and impure BIF samples and to
205 determine endmember for the detrital fraction and for the seawater-derived fraction
206 (Viehmann et al., 2015a).
207
208 5. Discussion

5.1 Decoupled Hf-Nd isotopes in the dissolved *and* the suspended fractions of Late Archean seawater

The *pure* chemical sediment endmember of the Krivoy Rog BIF (FUM57), representing the dissolved fraction (< 0.2 μm) of Krivoy Rog seawater that is composed of a mixture of seawater- and of hydrothermally-derived elements (Viehmann et al., 2015a), corroborates the findings of Viehmann et al. (2014) for Late Archean Temagami seawater. The Hf and Nd isotope systems in the dissolved fraction of the Krivoy Rog seawater are decoupled (Figure 3), suggesting that incongruent Hf release from the Krivoy Rog hinterland led to decoupling of Hf-Nd isotope systems in ambient Neoarchean seawater similar to modern Earth in which the 'seawater array' (after Albarede et al., 1998; Figure 3) resembles the Hf-Nd isotopic compositions of modern seawater and modern to Cenozoic seawater precipitates. Because decoupling of Hf-Nd isotopes in Late Archean seawater is now observed in marine chemical sediments from two near-contemporaneous deposits, we suggest that Hf-Nd decoupling in Late Archean seawater was a *global* rather than a local phenomenon in Neoarchean oceans. This observation further confirms that incongruent Hf weathering of zircon-bearing emerged crust was already a common process on Neoarchean Earth.

The Krivoy Rog schist, i.e. the most likely detrital endmember, is dominated by TTGs from the Krivoy Rog hinterland with a minor amphibolite component (Viehmann et al., 2015a) and shows a Zr concentration (138 ppm) which is two orders of magnitude higher than that of the Krivoy Rog BIF samples. The schist plots in εNd-εHf space slightly below the terrestrial array ('terrestrial array' after Vervoort et al., 1999, Figure 3). This relationship is commonly observed in (meta) igneous rocks of Phanerozoic and Precambrian age and indicates that the analyzed schist most closely resembles the average geochemical composition of the continental hinterland in the Krivoy Rog area.

The initial εNd and εHf values of *impure* BIFs, representing the geochemical budget composed of terrigenous and seawater-derived elements, are expected to plot along a

conservative two component mixing line between the detrital endmember (schist) with $\varepsilon Nd_{2.60Ga}$ and $\varepsilon Hf_{2.60Ga}$ of -4.0 and -8.06, respectively, and the pure chemical sediment endmember with $\varepsilon Nd_{2.60Ga}$ and $\varepsilon Hf_{2.60Ga}$ of -2.3 and +9.5, respectively. However, the $\varepsilon Nd_{2.60Ga}$ *and* $\varepsilon Hf_{2.60Ga}$ values of the impure Krivoy Rog BIFs do not plot between these endmember (Figure 3), show no correlation between their $\varepsilon Nd_{2.60Ga}$ and $\varepsilon Hf_{2.60Ga}$ values (r^2= 0.05), and yield systematically more positive $\varepsilon Nd_{2.60Ga}$ (and to some extend $\varepsilon Hf_{2.60Ga}$) values than the pure chemical sediment endmember (Figure 3, Table 1). Hence, this εHf-εNd decoupling in impure BIFs suggests that average clastic material from the Krivoy Rog hinterland does not predominantly control the isotope budget of the detrital component present in the impure Krivoy Rog BIF samples. Viehmann et al. (2014) used the relationship of Zr/Hf ratios in ancient marine chemical sediments as analogue to modern seawater because Zr/Hf ratios typically increase from coastal to open ocean seawater due to preferential sorption of Hf over Zr onto particulate Fe- and Mn-(oxyhydr)oxide surfaces (e.g. Godfrey et al., 1996; Schmidt et al., 2014) to distinguish impure, aluminosilicate-contaminated 2.7 Ga old Temagami BIF samples with near-chondritic Zr/Hf ratios ($Zr/Hf_{chondrite}$ = 34.3; after Münker et al., 2003) from pure chemical sediments with sub- and super-chondritic Zr/Hf ratios, which carry exclusively seawater-derived Hf. The impure BIF samples show sub-, super- and near-chondritic Zr/Hf ratios independent of their mineralogy (Table 1). Lack of correlations between Zr/Hf ratios with Hf concentrations (Figure 4, r^2 = 0.12) and with $\varepsilon Hf_{2.60Ga}$ (Figure 5, r^2 = 0.32) in the BIFs corroborates that simple two-component mixing between a detrital and chemical sediment endmember (i.e. seawater endmember) cannot explain the $\varepsilon Hf_{2.60Ga}$ values in the Krivoy Rog BIF. Furthermore, the individual Krivoy Rog BIF sample mineralogy is also not suitable to explain the specific Zr-Hf relationship similarly to reported alternating Si- and Fe-rich Temagami BIF samples with sub- and super-chondritic Zr/Hf ratios (Viehmann et al., 2014) and to Si-rich clastic sediments from the ~ 3.2 Ga old Barberton Greenstone Belt with strong radiogenic $\varepsilon Hf_{2.60Ga}$ values (Garcon et al., 2017), respectively.

5.2 The origin of Nd and Hf in Krivoy Rog BIFs

The Nd isotopic composition of the Krivoy Rog schist, i.e. detrital endmember, represents a mixture dominated by basement TTGs with minor amphibolites, while the chemical sediment endmember represents a mixture of dissolved terrigenous, continental crust-like, and mantle-like Nd hydrothermally derived from the oceanic crust, which shifts the $\varepsilon Nd_{2.60Ga}$ value of the chemical sediment to more positive values relative to the schist (Viehmann et al., 2015a). However, impure Krivoy Rog BIF samples show even more positive $\varepsilon Nd_{2.60Ga}$ than ambient seawater, suggesting that a more radiogenic, possibly more (ultra)mafic, detrital component with $\varepsilon Nd_{2.60Ga} >0$ additionally contributed to the geochemical budget of the marine chemical sediments (Viehmann et al., 2015a).

The source of dissolved Hf in seawater is more difficult to track due to analytical difficulties of Hf geochemistry in aqueous systems and the resulting scarcity of available studies. White et al. (1986) and Bau & Koschinsky (2006) described a potential hydrothermal pathway for dissolved Hf into seawater to explain Hf-Nd isotope decoupling, as riverine particulate and dissolved Hf would quantitatively be scavenged during estuarine processes. Most recent studies (Merschel et al., 2017a) revealed that riverine truly dissolved particle-reactive elements and those associated with organic (nano)particles may pass the estuarine system and may effectively contribute to the geochemical budget of the oceans, which supports the hypothesis that the 'zircon effect' may be responsible for the partial decoupling of both isotope systems in modern (e.g. Rickli et al., 2009; Zimmermann et al., 2009, Stichel et al. 2012), Cenozoic (e.g. van de Flierdt et al., 2004) and Late Archean oceans (Viehmann et al., 2014). Although from mass balance considerations, the ‘zircon effect’ has the highest impact on incongruent Hf release from continents (e.g., van de Flierdt et al., 2007), accessory minerals with high Lu/Hf ratios such as garnets, carbonates or phosphates may also have significant impact on the Hf isotopic composition of freshwaters in specific environments as

observed in sub-glacial rivers with low water-rock interaction times in West Greenland (Rickli et al., 2017), for example. Garcon et al. (2013; 2014b) observed a fractionation of εNd-εHf in bedload and suspended load in modern river systems on the continental hinterland. Similar to aeolian sorting which allows for long transportation distances for the finest sediment particles (e.g., Albarede et al., 1998; Pettke et al., 2002), hydrodynamical mineral sorting separates sand-sized zircon-bearing fractions that settle early into the bedload from finer grained particles that remain in the suspended load and may travel over longer distances (Garcon et al., 2013). Hence, the sand-sized fraction with high abundance of zircons and unradiogenic Hf isotope composition is mostly deposited close to the drainage area and proximal to the river outflow, while suspended material (e.g., phyllosilicates such as clay minerals, mica, and chlorite) with more radiogenic Hf isotopic compositions may reach more distal deltaic or estuarine parts. In systems rich in organic particles only a small fraction (e.g. Boyle et al., 1977; Merschel et al., 2017b) of the suspended particles and colloids gets trapped in the estuary due to the 'salting out effect' (surface charge transformation of colloids due to increasing salinity leads to coagulation and flocculation), while the remaining ones may enter the oceans. In marked contrast, in systems dominated by inorganic particles, which are the most likely analogue for Archean settings, more than 98% of the suspended material gets trapped in the estuary (Pokrovsky et al., 2014; Tepe and Bau, 2016). However, the impact of particles which are exported across the estuary and enter the open ocean, on the Hf isotopic composition of the dissolved fraction of (ancient) seawater is barely understood yet. Although some studies suggest that boundary exchange processes between sediment and seawater are a possible mechanism to explain the radiogenic Hf isotopic composition of seawater (e.g., Chen et al., 2013; Rickli et al., 2014), the mechanisms behind these processes are not known. Hence, as long as these mechanisms are not understood, we have to presume that suspended Hf and its isotope composition should be only be relevant for detrital material based on the high particle-reactivity and short residence time of Hf in seawater.

While the 'zircon effect' and significant weathering of accessory minerals with high Lu/Hf (e.g., garnets, phosphates, carbonates) may result in decoupling of Hf-Nd isotopes in local seawater and heterogeneous εHf values that are controlled by the individual mineralogy and composition of the weathered continental hinterland, the slightly different residence times of Hf and Nd in seawater may also decouple both the Hf and Nd isotope systems. In modern seawater, the residence time of Hf is slightly shorter than that of Nd with less than 500 years which is shorter than time which is needed to homogenize the isotopic compositions of the global oceans (Tachikawa et al., 1999; Siddall et al. 2008; Filippova et al., 2017). For the Archean time, however, the residence times of Hf and Nd in predominantly anoxic seawater are not well constrained. Because the Archean oceans were likely in Fe^{2+}-rich, Fe(oxy)hydroxides should have been the main scavenger for particle reactive elements in local water masses from which the BIFs precipitated. Different residence times of Hf and Nd had of course only an impact on their isotopic compositions in Archean seawater, if particle reactive elements have not been quantitatively scavenged from water masses during oxidation, which is one proposed model to explain the deposition of BIFs (e.g., Morris, 1993). However, it has been reported that the residence time of Nd was probably somewhat longer in Archean seawater relative to modern oceans, but it was shorter than the mixing time which is needed to homogenize the global Archean oceans (Alexander et al., 2009; Viehmann et al., 2015a). Since the same process would have affected the behavior of particle reactive Hf, it can be expected that the residence time of Hf in *Archean* seawater was also shorter than that of Nd. Hence, we speculate that a true decoupling of the Hf-Nd isotope systems in particle- and Fe(oxy)hydroxide-rich Archean seawater may have been produced independently from the 'zircon effect' and the mineralogy of the continental hinterland.

In essence and independent of very local mineralogical controls, the initial εHf values in aqueous systems increase from (i) zircon-bearing, coarse-grained sediment to (ii) zircon-free, fine-grained sediment/particulates to (iii) the dissolved fraction (nanoparticles and

colloids) to (iv) the truly dissolved fraction. Applying this relationship to the Krivoy Rog samples, the schist should most closely represent the (i) zircon-bearing coarse grained sediment, while the impure BIF samples should represent a mixture between the (ii) and (iii) fractions, and the pure chemical sediment endmember should fall into the range between the (iii) and (iv) fractions. However, this expectation is not met by the Krivoy Rog data set in which the $\varepsilon Hf_{2.60Ga}$ values of the chemical sediment endmember are similar to or less radiogenic than those of most impure BIF samples (Figure 3). We, therefore, suggest that the very positive and variable $\varepsilon Hf_{2.60Ga}$ values of impure Krivoy Rog BIFs are the result of contamination by very fine-grained particles with very radiogenic Hf isotope compositions relative to the eroded bulk material and were controlled by the mineralogy of the contaminant. The most likely source for the fine-grained particles are young volcanic ashes or wind-blown, zircon-free (ultra)mafic aeolian particles (see illustration in Figure 3). We further propose that wind-blown particles provide the most likely explanation for the decoupling of the Hf-Nd isotope systems in the impure Krivoy Rog BIFs, because:

1. Suspended riverine particles with radiogenic Hf isotopic compositions as observed in modern systems (Garcon et al., 2013) are an unlikely contaminant for the impure Krivoy Rog BIF, because almost all dissolved (colloidal + nanoparticulate) and particulate particle-reactive elements (including Hf) get quantitatively trapped in inorganic estuarine systems (Tepe and Bau, 2016) which are the most likely modern analogues to Archean settings.

2. In contrast to other Archean BIFs that show sedimentological and/or geochemical evidence for a near-shore or 'shallow-water' depositional environment such as the Pongola or Witwatersrand BIFs (e.g., Beukes & Cairncross, 1991; Alexander et al. 2008; Smith et al., 2013; Viehmann et al., 2015b), there is no such evidence for the Krivoy Rog BIFs. Sedimentology and trace element geochemistry combined with Nd isotopes rather suggest that the Krivoy Rog BIF depositional environment was a restricted basin comparable to the

364 modern Baltic Sea (Kulik and Korzhnev, 1997) that had only limited connection to global
365 Late Archean oceans (Kulik 1991; Viehmann et al., 2015a).

366 3. The offset in $\varepsilon Nd_{2.60Ga}$ values in impure BIFs relative to the detrital and chemical
367 sediment endmember can also only be explained by a contaminant characterized by a more
368 radiogenic component with very positive $\varepsilon Nd_{2.60Ga}$ values.

369 The less radiogenic $\varepsilon Hf_{2.60Ga}$ value in the chemical sediment endmember relative to
370 impure BIF samples (see illustration in Figure 3) can be explained by two different scenarios
371 or a combination of both. First, a hydrothermal Hf pathway via black smoker-style, high-
372 temperature hydrothermal fluids into ancient Krivoy Rog seawater, analogous to the
373 hydrothermal REY pathway that is commonly reported for Archean BIFs (e.g., Danielson et
374 al., 1991; Viehmann et al., 2015a), also existed in Late Archean oceans. In this scenario,
375 direct Hf scavenging processes in anoxic Archean seawater close to the venting sites was
376 prevented and the hydrothermal Hf could travel longer distances than in the oxidized modern
377 oceans. Hence, this hydrothermal Hf should also have had a significant impact on the
378 dissolved Hf budget of Archean seawater. Second, the Hf-Nd isotope systems in the dissolved
379 fraction of Krivoy Rog seawater are truly decoupled based on different residence times of Hf
380 and Nd, i.e. independently of the mineralogical composition of the weathered hinterland rocks.
381 However, the decoupling of the εHf-εNd values in Krivoy Rog seawater of both (combined?)
382 scenarios is less pronounced than the εHf-εNd decoupling due incongruent Hf weathering of
383 the continental hinterland and the 'zircon effect' which produced even more radiogenic, but
384 heterogeneous Hf input into ancient seawater. These combined effects resulted in less positive
385 $\varepsilon Hf_{2.60Ga}$ values of the truly dissolved and the dissolved Hf fractions of Archean seawater
386 (represented by the pure chemical sediment endmember).

387

388 5.3 Influence of weathered and eroded (ultra)mafic material on the Nd isotopes in Archean
389 waters

Neodymium isotopes in clastic sediments are a reliable tracer for provenance studies due to congruent Nd weathering on the continents and rather similar Nd isotope compositions of different grain-size fractions of clastic sediments (e.g. Patchett et al., 1984; Garcon et al., 2013; Garcon et al., 2017). However, Garcon et al. (2014a) studied particles of the suspended and bedload fractions in modern rivers that drain crystalline continental basement and high amounts of basaltic floodplains. The authors observed a shift of up to 6 εNd units between the bedload which is dominated by coarse-grained crystalline material (e.g., quartz, zircons), and the suspended load that is predominantly comprised of fine-grained weathered basaltic material (e.g., phyllosilicates). This results in an overestimate of the importance of the suspended basaltic components in the riverine input into the estuarine system, relative to bulk weathering products. The presence and overrepresentation of (ultra)mafic terrigenous material is also reflected in the $\varepsilon Nd_{2.60Ga}$ values of impure Krivoy Rog BIFs with higher $\varepsilon Nd_{2.60Ga}$ values that are 1 to 2 units higher than the chemical sediment endmember and 3 to 4 units higher than the weathered bulk material. Similar to the observation in the Krivoy Rog BIF, detritus-contaminated Archean BIF samples of the 'shallow-water' Witwatersrand BIF (Viehmann et al., 2015b) also show initial εNd values that are more positive than the associated seawater endmember. Based on the observation of Garcon et al. (2014a) made in modern river systems, we suggest that the more positive initial εNd values reported for impure Archean BIF samples may be related to the overrepresentation of weathered and eroded, fine-grained (ultra)mafic material that shifts the εNd values of impure Archean BIFs to more positive values. This observation is in agreement with the widely accepted view that the composition of the emerged Archean crust which was exposed to subaerial weathering and erosion processes, consisted of higher abundances of (ultra)mafic rocks relative to modern continental crust (e.g. Kamber, 2010; Kamber, 2015). However, the overrepresentation of weathered (ultra)mafic terrigenous material in Archean rivers and oceans is based on the assumption that both (ultra)mafic and more evolved rocks were present

in the river catchment areas to separate weathering-resistant, sand-sized 'felsic' minerals and (ultra)mafic fine-grained minerals (e.g., phyllosilicates). Thus, weathering of (ultra)mafic Archean crust did not only have a major impact on the dissolved seawater chemistry and on the trace element systematics of Archean oceans (Kamber et al., 2010), but also on the suspended loads delivered by rivers to Archean estuaries and coastal seas and by dust-blown particles into open-ocean settings. Over-representation of fine grained suspended (ultra)mafic loads relative to bulk weathering products that were delivered into ancient seawater via rivers or aeolian processes may further lead to misinterpretation of Nd isotope provenance studies of Archean clastic sediments that are exclusively based on very fine-grained, zircon-free loads. These findings also highlight the importance of careful evaluation of detrital contamination in marine chemical sediments for their use as reliable seawater archives, because even small amounts of fine-grained clastic material may have significant impact on the isotope budget of chemical sediments.

6. Conclusions

The unique potential of coupled Hf-Nd isotope studies of pure and impure Archean marine chemical sediments allows us to evaluate weathering and erosion processes on early Earth. Pure and impure (i.e. detritus-rich) BIF samples from the Neoarchean Krivoy Rog BIF yield calculated Sm-Nd and Lu-Hf ages that overlap within the error of the published depositional age, suggesting negligible post-depositional alterations of both isotope systems. However, both isochrons represent mixing lines between a detrital and a seawater endmember, and yield only limited geochronological information.

The *pure* BIF samples which represent the local Krivoy Rog seawater endmember, confirm decoupling of the Hf-Nd isotope systems in the dissolved pool of Late Archean seawater and corroborate the findings of Viehmann et al. (2014) who observed similar decoupling of the Hf-Nd isotope systems in ~2.7 Ga Temagami seawater. This suggests that

442 incongruent release of Hf during terrestrial weathering and erosion of zircon-bearing emerged
443 crust were probably a *global* and not only a local phenomenon during the Late Archean.
444 *Impure* BIFs from Krivoy Rog, which are composed of a mixture of detrital and
445 seawater-derived components, show a similar decoupling of the Hf-Nd isotope systems. We
446 here showed for the first time that hydrodynamical and aeolian mineral sorting and separation
447 of unradiogenic zircon-bearing sand-sized fractions from fine-grained zircon-free fractions
448 and/or accessory minerals with high Lu/Hf ratios already operated on/in Late Archean
449 continents, rivers and oceans. The very positive, but variable $\varepsilon Hf_{2.60Ga}$ values of impure BIFs
450 result from a mineralogical control of the weathered continental material, i.e. from the co-
451 deposition of radiogenic zircon-free fine-grained suspended particles and marine chemical
452 sediments. Less positive $\varepsilon Hf_{2.60Ga}$ values in the dissolved seawater fraction relative to impure
453 BIF samples point either towards a hydrothermal Hf pathway via black smoker-style high-
454 temperature hydrothermal fluids into anoxic Archean seawater and/or Hf-Nd isotope
455 decoupling in Archean seawater based on different residence times of Hf and Nd in
456 Neoarchean oceans. Furthermore, the generally more positive $\varepsilon Nd_{(i)}$ values of impure Archean
457 BIFs relative to pure ones (representing seawater) support the idea that weathering and
458 erosion of (ultra)mafic material (e.g., phyllosilicates (clay minerals, mica, and chlorite)) made
459 a significant impact on the suspended loads and the overall seawater chemistry of Archean
460 oceans.
461
462 Acknowledgements
463 We strongly acknowledge the generosity and help of Dimitrii Kulik who provided the Krivoy
464 Rog samples to M.B.. S.V. and M.B. acknowledge the support from Jacobs University
465 Bremen for a temporary Ph.D. scholarship for S.V. S.V. especially thanks Nathalie Tepe for
466 discussions of elemental behavior during estuarine processes and Katja Schmidt for fruitful
467 discussions about the Hf-Nd isotope systems in aqueous systems. We also want to

468 acknowledge Catherine Chauvel for her editorial handling and two anonymous reviewers for
469 their positive and constructive comments which helped to improve the final version of the
470 manuscript. This study was partially funded by the Horizon 2020 Marie Curie Individual
471 Fellowship to S.V. and is related to the SPP 1833 "Building a Habitable Earth".

472

473 References

474 Albarède, F., Simonetti, A., Vervoort, J.D., Blichert-Toft, J., Abouchami, W., 1998. A Hf-Nd
475 isotopic correlation in ferromanganese nodules. Geophys. Res. Lett. 25, 3895–3898.
476 doi:10.1029/1998GL900008

477 Alexander, B.W., 2008. Trace element analyses in geological materials using low resolution
478 inductively coupled plasma mass spectrometry (ICPMS) Technical Report No . 18
479 School of Engineering and Science.

480 Alexander, B.W., Bau, M., Andersson, P., Dulski, P., 2008. Continentally-derived solutes in
481 shallow Archean seawater: Rare earth element and Nd isotope evidence in iron formation
482 from the 2.9Ga Pongola Supergroup, South Africa. Geochim. Cosmochim. Acta 72,
483 378–394. doi:10.1016/j.gca.2007.10.028

484 Alexander, B.W., Bau, M., Andersson, P., 2009. Neodymium isotopes in Archean seawater
485 and implications for the marine Nd cycle in Earth's early oceans. Earth Planet. Sci. Lett.
486 283, 144–155. doi:10.1016/j.epsl.2009.04.004

487 Alibert, C., McCulloch, M.T., 1993. Rare earth element and neodymium isotopic
488 compositions of the banded iron-formations and associated shales from Hamersley,
489 Western Australia. Geochim. Cosmochim. Acta 57, 187–204.

490 Bau, M., Alexander, B.W., 2009. Distribution of high field strength elements (Y, Zr, REE, Hf,
491 Ta, Th, U) in adjacent magnetite and chert bands and in reference standards FeR-3 and
492 FeR-4 from the Temagami iron-formation, Canada, and the redox level of the
493 Neoarchean ocean. Precambrian Res. 174, 337–346.
494 doi:10.1016/j.precamres.2009.08.007

495 Bau, M., Dulski, P., 1996. Distribution of yttrium and rare-earth elements in the Penge and
496 Kuruman iron-formations, Transvaal Supergroup, South Africa. Precambrian Res. 79,
497 37–55. doi:10.1016/0301-9268(95)00087-9

498 Bau, M., Koschinsky, A., 2006. Hafnium and neodymium isotopes in seawater and in
499 ferromanganese crusts: The "element perspective." Earth Planet. Sci. Lett. 241, 952–961.
500 doi:10.1016/j.epsl.2005.09.067

501 Bayon, G., Vigier, N., Burton, K.W., Jean Carignan, A.B., Etoubleau, J., Chu, N.-C., 2006.
502 The control of weathering processes on riverine and seawater hafnium isotope ratios.
503 Geology 34, 433. doi:10.1130/G22130.1

Bayon, G., Skonieczny, C., Delvigne, C., Toucanne, S., Bermell, S., Ponzevera, E., André, L., 2016. Environmental Hf–Nd isotopic decoupling in World river clays. Earth Planet. Sci. Lett. 438, 25–36. doi:10.1016/j.epsl.2016.01.010

Bekker, A., Slack, J.F., Planavsky, N., Krapež, B., Hofmann, A., Konhauser, K.O., Rouxel, O.J., 2010. Iron formation: The sedimentary product of a complex interplay among mantle, tectonic, oceanic, and biospheric processes. Econ. Geol. 105, 467–508. doi:10.2113/gsecongeo.105.3.467

Beukes, N.J., Cairncross, B., 1991. A lithostratigraphic-sedimentological reference profile for the Late Archean Mozaan Group, Pongola Sequence: Application to sequence stratigraphy and correlation with the Witwatersrand Supergroup. South African Journal of Geology 94, 44-69.

.Bibikova, E. V., Claesson, S., Fedotova, A. A., Artemenko, G. V., Il'inskii, L., 2010. Terrigenous zircon of archean greenstone belts as a source of information on the 's crust: Azov and Dnieper domains, Ukrainian shield. Geochemistry Int. 48, 845–861.

Bouvier, A., Vervoort, J.D., Patchett, P.J., 2008. The Lu–Hf and Sm–Nd isotopic composition of CHUR: Constraints from unequilibrated chondrites and implications for the bulk composition of terrestrial planets. Earth Planet. Sci. Lett. 273, 48–57. doi:10.1016/j.epsl.2008.06.010

Chen, T. Y., Li, G., Frank, M., & Ling, H. F. (2013). Hafnium isotope fractionation during continental weathering: Implications for the generation of the seawater Nd-Hf isotope relationships. *Geophysical Research Letters*, *40*(5), 916–920. https://doi.org/10.1002/grl.50217

Danielson, A., Möller, P., Dulski, P., 1992. The europium anomalies in banded iron formations and the thermal history of the oceanic crust. Chem. Geol. 97, 89–100.

Filippova, A., Frank, M., Kienast, M., Rickli, J., Hathorne, E., Yashayaev, I. M., & Pahnke, K. (2017). Water mass circulation and weathering inputs in the Labrador Sea based on coupled Hf–Nd isotope compositions and rare earth element distributions. *Geochimica et Cosmochimica Acta*, *199*, 164–184. https://doi.org/10.1016/j.gca.2016.11.024

Fryer, B.J., Fyfe, W.S., Kerrich, R., 1979. Archaean volcanogenic oceans. Chem. Geol. 24, 25–33.

Garçon, M., Chauvel, C., France-Lanord, C., Huyghe, P., Lavé, J., 2013. Continental sedimentary processes decouple Nd and Hf isotopes. Geochim. Cosmochim. Acta. doi:10.1016/j.gca.2013.07.027

Garçon, M., Chauvel, C., 2014a. Where is basalt in river sediments, and why does it matter? Earth Planet. Sci. Lett. 407, 61–69. doi:10.1016/j.epsl.2014.09.033

Garçon, M., Chauvel, C., France-Lanord, C., Limonta, M., Garzanti, E., 2014b. Which minerals control the Nd–Hf–Sr–Pb isotopic compositions of river sediments? Chem. Geol. 364, 42–55. doi:10.1016/j.chemgeo.2013.11.018

Garçon, M., Carlson, R.W., Shirey, S.B., Arndt, N.T., Horan, M.F., Mock, T.D., 2017. Erosion of Archean continents: The Sm-Nd and Lu-Hf isotopic record of Barberton sedimentary rocks. Geochim. Cosmochim. Acta 206, 216–235. doi:10.1016/j.gca.2017.03.006

German, C.R., Klinkhammer, G.P., Edmond, J.M., Mitra, A., Elderfield, H., 1990. Hydrothermal scavenging of rare earth elements in the ocean. Nature 345, 516–518.

Godfrey, L.V., White, W.M., Salters, V.J.M., 1996. Dissolved zirconium and hafnium distributions across a shelf break in the northeastern Atlantic Ocean. Geochim. Cosmochim. Acta 60, 3995–4006. doi:10.1016/S0016-7037(96)00246-3

Godfrey, L. V., Zimmermann, B., Lee, D. C., King, R. L., Vervoort, J. D., Sherrell, R. M., & Halliday, A. N. (2009). Hafnium and neodymium isotope variations in NE Atlantic seawater. *Geochemistry, Geophysics, Geosystems*, *10*(8), 1–13. https://doi.org/10.1029/2009GC002508

Hoffmann, J.E., Münker, C., Polat, A., Rosing, M.T., Schulz, T., 2011. The origin of decoupled Hf–Nd isotope compositions in Eoarchean rocks from southern West Greenland. Geochim. Cosmochim. Acta 75, 6610–6628. doi:10.1016/j.gca.2011.08.018

Hoffmann, J.E., Kröner, A., Hegner, E., Viehmann, S., Xie, H., Iaccheri, L.M., Schneider, K.P., Hofmann, A., Wong, J., Geng, H., Yang, J., 2016. Source composition, fractional crystallization and magma mixing processes in the 3.48 - 3.43 Ga Tsawela tonalite suite (Ancient Gneiss Complex, Swaziland)–implications for Palaeoarchaean geodynamics. Precambrian Res. doi:10.1016/j.precamres.2016.01.026

Kamber, B.S., 2010. Archean mafic–ultramafic volcanic landmasses and their effect on ocean–atmosphere chemistry. Chem. Geol. 274, 19–28. doi:10.1016/j.chemgeo.2010.03.009

Kamber, B.S., 2015. The evolving nature of terrestrial crust from the Hadean, through the Archaean, into the Proterozoic. Precambrian Res. 258, 48–82. doi:10.1016/j.precamres.2014.12.007

Kulik, D.A., 1991. Rhythmical banding as reflection of conditions of sedimentation and diagenetic transformation of banded iron formation rocks. In: Kravchenko, V.M. and Kulik, D.A. (eds), Precambrian iron formations of the European part of the USSR, Naukova Dumka, Kiev, 22-42 (in Russian).

Kulik, D.A., Korzhnev, M.N., 1997. Lithological and geochemical evidence of Fe and Mn pathways during deposition of Lower Proterozoic banded iron formation in the Krivoy Rog Basin (Ukraine). Geol. Soc. London, Spec. Publ.

Li, W., Beard, B.L., Johnson, C.M., 2015. Biologically recycled continental iron is a major component in banded iron formations. PNAS 112, 8193–8198. doi:10.1073/pnas.1505515112

Lugmair, G.W., Marti, K., 1978. Lunar initial 143Nd/144Nd: Differential evolution of the lunar crust and mantle. Earth Planet. Sci. Lett. 39, 349–357.

581 Merschel, G., Bau, M., & Dantas, E. L. 2017a. Contrasting impact of organic and inorganic
582 nanoparticles and colloids on the behavior of particle-reactive elements in tropical
583 estuaries: An experimental study. Geochimica et Cosmochimica Acta, *197*, 1–13.
584 https://doi.org/10.1016/j.gca.2016.09.041

585 Merschel, G., Bau, M., Schmidt, K., Münker, C., Dantas, E.L., 2017b. Hafnium and
586 neodymium isotopes and REY distribution in the truly dissolved, colloidal and
587 particulate loads of the Amazon basin, Brazil. Geochim. Cosmochim. Acta

588 Miller, R.G., O´Nions, R.K., 1985. Source of Precambrian chemical and clastic sediments.
589 Nature 314, 325–330.

590 Morris, R., 1993. Genetic modelling for banded iron-formation of the Hamersley Group,
591 Pilbara Craton, Western Australia. Precambrian Res. 60, 243–286.

592 Münker, C., Weyer, S., Scherer, E., Mezger, K., 2001. Separation of high field strength
593 elements (Nb, Ta, Zr, Hf) and Lu from rock samples for MC-ICPMS measurements.
594 Geochemistry, Geophys. Geosystems 2, n/a–n/a. doi:10.1029/2001GC000183

595 Münker, C., Pfänder, J. A, Weyer, S., Büchl, A., Kleine, T., Mezger, K., 2003. Evolution of
596 planetary cores and the Earth-Moon system from Nb/Ta systematics. Science 301, 84–87.
597 doi:10.1126/science.1084662

598 Patchett, P.J., White, W.M., Feldmann, H., Kielinczuk, S., Hofmann, a. W., 1984.
599 Hafnium/rare earth element fractionation in the sedimentary system and crustal recycling
600 into the Earth's mantle. Earth Planet. Sci. Lett. 69, 365–378. doi:10.1016/0012-
601 821X(84)90195-X

602 Pettke, T., Lee, D.C., Halliday, A.N., Rea, D.K., 2002. Radiogenic Hf isotopic compositions
603 of continental eolian dust from Asia, its variability and its implications for seawater Hf.
604 Earth Planet. Sci. Lett. 202, 453–464. doi:10.1016/S0012-821X(02)00778-1

605 Piepgras, D.J., Wasserburg, G.J., 1980. Neodymium isotopic variations in seawater. Earth
606 Planet. Sci. Lett. 50, 128–138. doi:10.1016/0012-821X(80)90124-7

607 Pin, C., Zalduegui, J.S., 1997. Sequential separation of light rare-earth elements, thorium and
608 uranium by miniaturized extraction chromatography: application to isotopic analyses of
609 silicate rocks. Analytica Chimica Acta, 339, 79-89.

610 Pokrovsky, O. S., Shirokova, L. S., Viers, J., Gordeev, V. V., Shevchenko, V. P., Chupakov,
611 A. V., … Zouiten, C. (2014). Fate of colloids during estuarine mixing in the Arctic.
612 *Ocean Science*, *10*(1), 107–125. https://doi.org/10.5194/os-10-107-2014

613 Rickli, J., Frank, M., Halliday, A.N., 2009. The hafnium-neodymium isotopic composition of
614 Atlantic seawater. Earth Planet. Sci. Lett. 280, 118–127. doi:10.1016/j.epsl.2009.01.026

615 Rickli, J., Frank, M., Stichel, T., Georg, R.B., Vance, D., Halliday, A.N., 2013. Controls on
616 the incongruent release of hafnium during weathering of metamorphic and sedimentary
617 catchments. Geochim. Cosmochim. Acta 101, 263–284. doi:10.1016/j.gca.2012.10.019

618 Scherer, E., Münker, C., Mezger, K., 2001. Calibration of the lutetium-hafnium clock.
619 Science (80-.). 293, 683–687. doi:10.1126/science.1061372

620 Schmidt, K., Bau, M., Hein, J., Koschinsky, A., 2014. Fractionation of the geochemical twins
621 Zr-Hf and Nb-Ta during scavenging from seawater by hydrogenetic ferromanganese
622 crusts. Geochim. Cosmochim. Acta. doi:10.1016/j.gca.2014.05.036

623 Shcherbak, N.P., Artamenko G.V., Barmitsky E.N. et al., 1989. Precambrian
624 geochronological scale of the Ukrainian Shield. Naukova Dumka, Kiev, 142 pp. (in
625 Russian).

626 Shcherbak, N.P., Bartnitsky, Ye.N., Bibikova, E.V., Boyko, V.L., 1984. Age and evolution of
627 the Early Precambrian continental crust of the Ukrainian Shield, in: Kröner, A. (Ed.),
628 Archean Geochemistry: the origin and evolution of the Archaean continental crust,
629 Springer, Berlin, pp. 251-261.

630 Siddall M., Khatiwala S., van de Flierdt T., Jones K., Goldstein S. L., Hemming S. and
631 Anderson R. F., 2008. Towards explaining the Nd paradox using reversible scavenging
632 in an ocean general circulation model. Earth Planet. Sci. Lett. 274, 448–461

633 Smith, A.J.B., Beukes, N.J., Gutzmer, J., 2013. The composition and depositional
634 environments of Mesoarchean iron formations of the West Rand Group of the
635 Witwatersrand Supergroup, South Africa. Econ. Geol. 108, 111–134.
636 doi:10.2113/econgeo.108.1.111

637 Söderlund, U., Patchett, P.J., Vervoort, J.D., Isachsen, C.E., 2004. The 176Lu decay constant
638 determined by Lu–Hf and U–Pb isotope systematics of Precambrian mafic intrusions.
639 Earth Planet. Sci. Lett. 219, 311–324. doi:10.1016/S0012-821X(04)00012-3

640 Stichel, T., Frank, M., Rickli, J., Hathorne, E.C., Haley, B. a., Jeandel, C., Pradoux, C., 2012.
641 Sources and input mechanisms of hafnium and neodymium in surface waters of the
642 Atlantic sector of the Southern Ocean. Geochim. Cosmochim. Acta 94, 22–37.
643 doi:10.1016/j.gca.2012.07.005

644 Szilas, K., Hoffmann, J.E., Hansmeier, C., Hollis, J.A., Münker, C., Viehmann, S., Kasper,
645 H.U., 2015. Sm-Nd and Lu-Hf isotope and trace-element systematics of Mesoarchaean
646 amphibolites, inner Ameralik fjord, southern West Greenland. Mineral. Mag. 79, 857–
647 876. doi:10.1180/minmag.2015.079.4.02

648 Szilas, K., Hoffmann, J. E., Schulz, T., Hansmeier, C., Polat, A., Viehmann, S., Kasper, H.U.,
649 Münker, C. 2016. Combined bulk-rock Hf- and Nd-isotope compositions of
650 Mesoarchaean metavolcanic rocks from the Ivisaartoq Supracrustal Belt, SW Greenland:
651 Deviations from the mantle array caused by crustal recycling. *Chemie Der Erde -*
652 *Geochemistry*, *76*(4), 543–554. http://doi.org/10.1016/j.chemer.2016.09.004

653 Tachikawa, K., Jeandel, C., Roy-Barman, M., 1999. A new approach to the Nd residence time
654 in the ocean: the role of atmospheric inputs. Earth Planet. Sci. Lett. 170, 433–446.
655 doi:10.1016/S0012-821X(99)00127-2

656 Tachikawa, K., Arsouze, T., Bayon, G., Bory, A., Colin, C., Dutay, J. C., … Waelbroeck, C.
657 (2017). The large-scale evolution of neodymium isotopic composition in the global

modern and Holocene ocean revealed from seawater and archive data. *Chemical Geology*, *457*(March), 131–148. https://doi.org/10.1016/j.chemgeo.2017.03.018

Tepe, N., Bau, M., 2016. Behavior of rare earth elements and yttrium during simulation of arctic estuarine mixing between glacial-fed river waters and seawater and the impact of inorganic (nano-)particles. Chem. Geol. 438, 134–145. doi:10.1016/j.chemgeo.2016.06.001

van De Flierdt, T., Frank, M., Lee, D.-C., Halliday, A.N., Reynolds, B.C., Hein, J.R., 2004. New constraints on the sources and behavior of neodymium and hafnium in seawater from Pacific Ocean ferromanganese crusts. Geochim. Cosmochim. Acta 68, 3827–3843. doi:10.1016/j.gca.2004.03.009

van de Flierdt, T., Goldstein, S.L., Hemming, S.R., Roy, M., Frank, M., Halliday, A.N., 2007. Global neodymium–hafnium isotope systematics — revisited. Earth Planet. Sci. Lett. 259, 432–441. doi:10.1016/j.epsl.2007.05.003

van de Flierdt, T., Griffiths, A. M., Lambelet, M., Little, S. H., Stichel, T., & Wilson, D. J. (2016). Neodymium in the oceans: a global database, a regional comparison and implications for palaeoceanographic research. *Philosophical Transactions of the Royal Society A: Mathematical, Physical and Engineering Sciences*, *374*(2081), 20150293. https://doi.org/10.1098/rsta.2015.0293

Vervoort, J.D., Patchett, P.J., Blichert-Toft, J., Albarede, F., 1999. Relationships between Lu – Hf and Sm – Nd isotopic systems in the global sedimentary system. Earth Planet. Sci. Lett. 168, 79–99.

Viehmann, S., Hoffmann, J.E., Münker, C., Bau, M., 2014. Decoupled Hf-Nd isotopes in Neoarchean seawater reveal weathering of emerged continents. Geology 42, 115–118. doi:10.1130/G35014.1

Viehmann, S., Bau, M., Hoffmann, J.E., Münker, C., 2015a. Geochemistry of the Krivoy Rog Banded Iron Formation, Ukraine, and the impact of peak episodes of increased global magmatic activity on the trace element composition of Precambrian seawater. Precambrian Res. 270, 165–180. doi:10.1016/j.precamres.2015.09.015

Viehmann, S., Bau, M., Smith, A.J.B., Beukes, N.J., Dantas, E.L., Bühn, B., 2015b. The reliability of ~2.9 Ga old Witwatersrand banded iron formations (South Africa) as archives for Mesoarchean seawater: Evidence from REE and Nd isotope systematics. J. African Earth Sci. 111, 322–334. doi:10.1016/j.jafrearsci.2015.08.013

Viehmann, S., Bau, M., Bühn, B., Dantas, E. L., Andrade, F. R. D., Walde, D. H. G. 2016. Geochemical characterisation of Neoproterozoic marine habitats: Evidence from trace elements and Nd isotopes in the Urucum iron and manganese formations, Brazil. *Precambrian Research*, *282*, 74–96. http://doi.org/10.1016/j.precamres.2016.07.006

Weyer, S., Münker, C., Rehkämper, M., 2002. Determination of ultra-low Nb , Ta , Zr and Hf concentrations and the chondritic Zr/Hf and Nb/Ta ratios by isotope dilution analyses with multiple collector ICP-MS 187, 295–313.

White, W.M., Patchett, J., BenOthman, D., 1986. Hf isotope ratios of marine sediments and Mn nodules: evidence for a mantle source of Hf in seawater. Earth Planet. Sci. Lett. 79, 46–54. doi:10.1016/0012-821X(86)90039-7

Zimmermann, B., Porcelli, D., Frank, M., Rickli, J., Lee, D.-C., Halliday, A.N., 2009. The hafnium isotope composition of Pacific Ocean water. Geochim. Cosmochim. Acta 73, 91–101. doi:10.1016/j.gca.2008.09.033

Figure Captions

Figure 1. Lutetium-Hf isochron of Krivoy Rog BIF samples. The Lu-Hf isochron of pure and impure BIF samples from the Neoarchean Krivoy Rog Supergroup overlaps within the error with the published Late Archean depositional age (Viehmann et al., 2015), strongly supporting negligible post-depositional alteration of the Hf isotope system. However, geochronological information are hampered due to the fact that the isochron is built up by pure BIFs with high $^{176}Lu/^{177}Hf$ and $^{176}Hf/^{177}Hf$ ratios and impure BIFs with respective lower ratios. This relationship indicates two component mixing rather than provides reliable information about the BIF depositional age. Note that the age calculation of the isochron was calculated without the shale. Error bars of individual samples are calculated by error propagation method.

Figure 2. Two component mixing of the Hf system between Krivoy Rog BIFs and the associated schist. Impure BIFs of the Krivoy Rog Supergroup plot between the chemical sediment and the detritus endmember, revealing a mixture of seawater-derived and detritus-derived Hf in the Late Archean marine chemical sediments.

Figure 3. Clastic and chemical sediments of the Krivoy Rog BIF in $\varepsilon Hf_{(i)}$ vs. $\varepsilon Nd_{(i)}$ space relative to the 'terrestrial' and 'seawater' arrays, the Temagami BIF and Asian eolian dust. While the Krivoy Rog schist shows a coupled behavior of the Hf-Nd isotope systems that is commonly observed in terrestrial magmatic systems, both the pure and detritus-contaminated

725 BIF samples of the Late Archean Krivoy Rog Supergroup yield a decoupling of both isotope
726 systems that is reported from modern aqueous systems and the Late Archean Temagami BIF
727 (Viehmann et al., 2014). The inlet illustrates a schematic explanation for the $\varepsilon Hf_{(i)}$ and. $\varepsilon Nd_{(i)}$
728 values found in the pure and impure Krivoy Rog BIF samples. Data for the terrestrial array,
729 seawater array, Asian eolian dust and Temagami BIF are taken from Vervoort et al. (1999),
730 Albarède et al. (1998), Pettke et al. (2002) and Viehmann et al. (2014), respectively. Error
731 bars are 2σ.
732
733 Figure 4. Plot of Zr/Hf ratios versus Hf concentrations of the BIFs relative to clastic
734 sediments from the Krivoy Rog area, the ~2.7 Ga old Temagami BIF and worldwide modern
735 river and seawater samples. The $Zr/Hf_{chondrite}$ ratio is taken from Münker et al. (2003). Note
736 that Hf concentrations of seawater and river water data are multiplied by 10^5.
737
738 Figure 5. Plot of Zr/Hf ratios versus $\varepsilon Hf_{(i)}$ of the Krivoy Rog BIFs and schist relative to the
739 ~2.7 Ga old Temagami BIF, chondrite, modern seawater and Asian eolian dust. Insignificant
740 correlations between Zr/Hf with Hf concentrations (Fig. 4, $r^2 = 0.12$) and $\varepsilon Hf_{(i)}$ values ($r^2 = 0.32$)
741 indicate that sample mineralogy and simple two-component mixing between a detrital and
742 chemical sediment endmember are not viable to explain the $\varepsilon Hf_{2.60Ga}$ values of the pure and
743 impure Krivoy Rog BIF. Errors are 2σ and smaller than the symbol size.
744

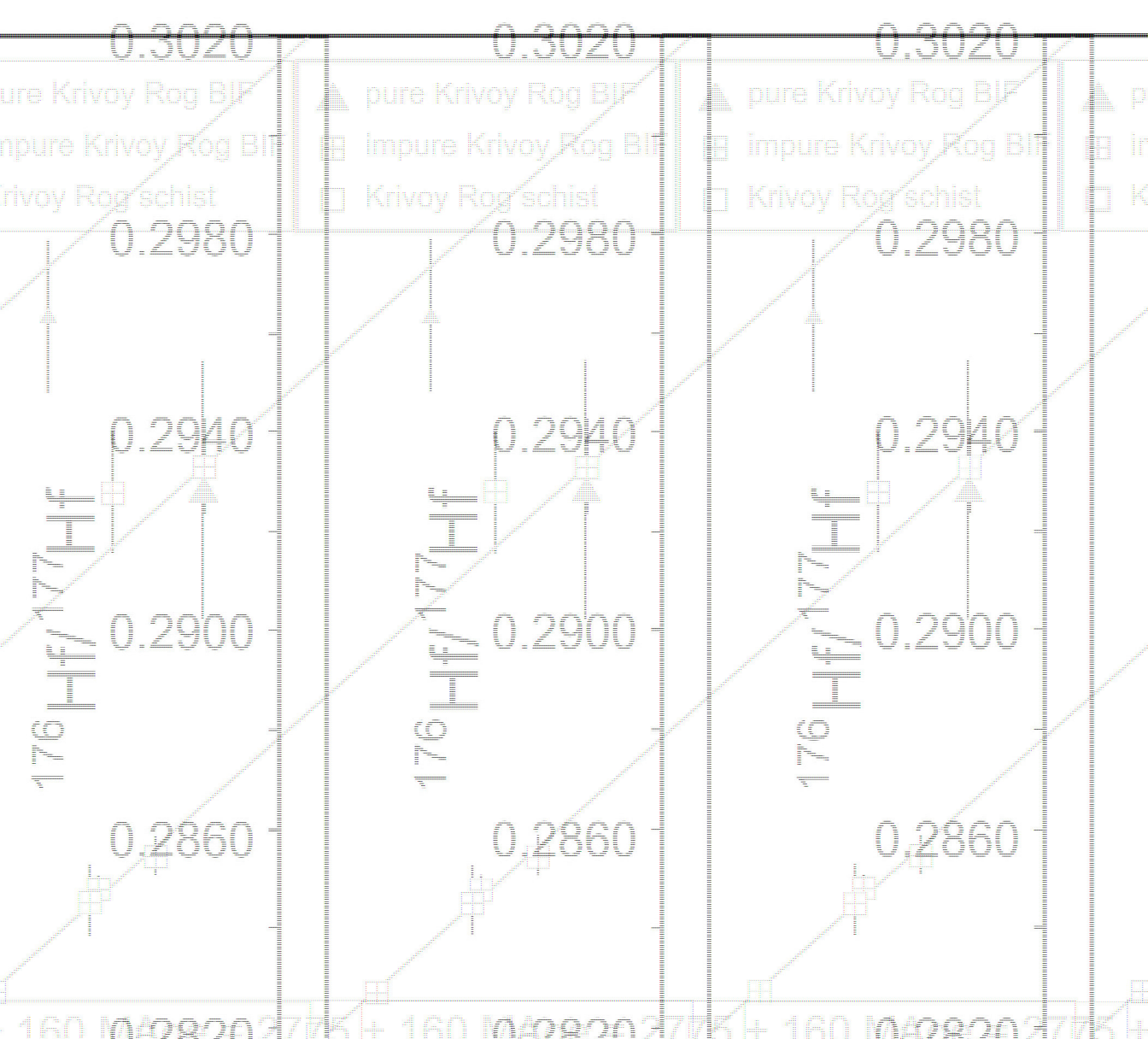
0.3020
0.2980
0.2940
0.2900
0.2860
pure Krivoy Rog BIF
impure Krivoy Rog BIF
Krivoy Rog schist

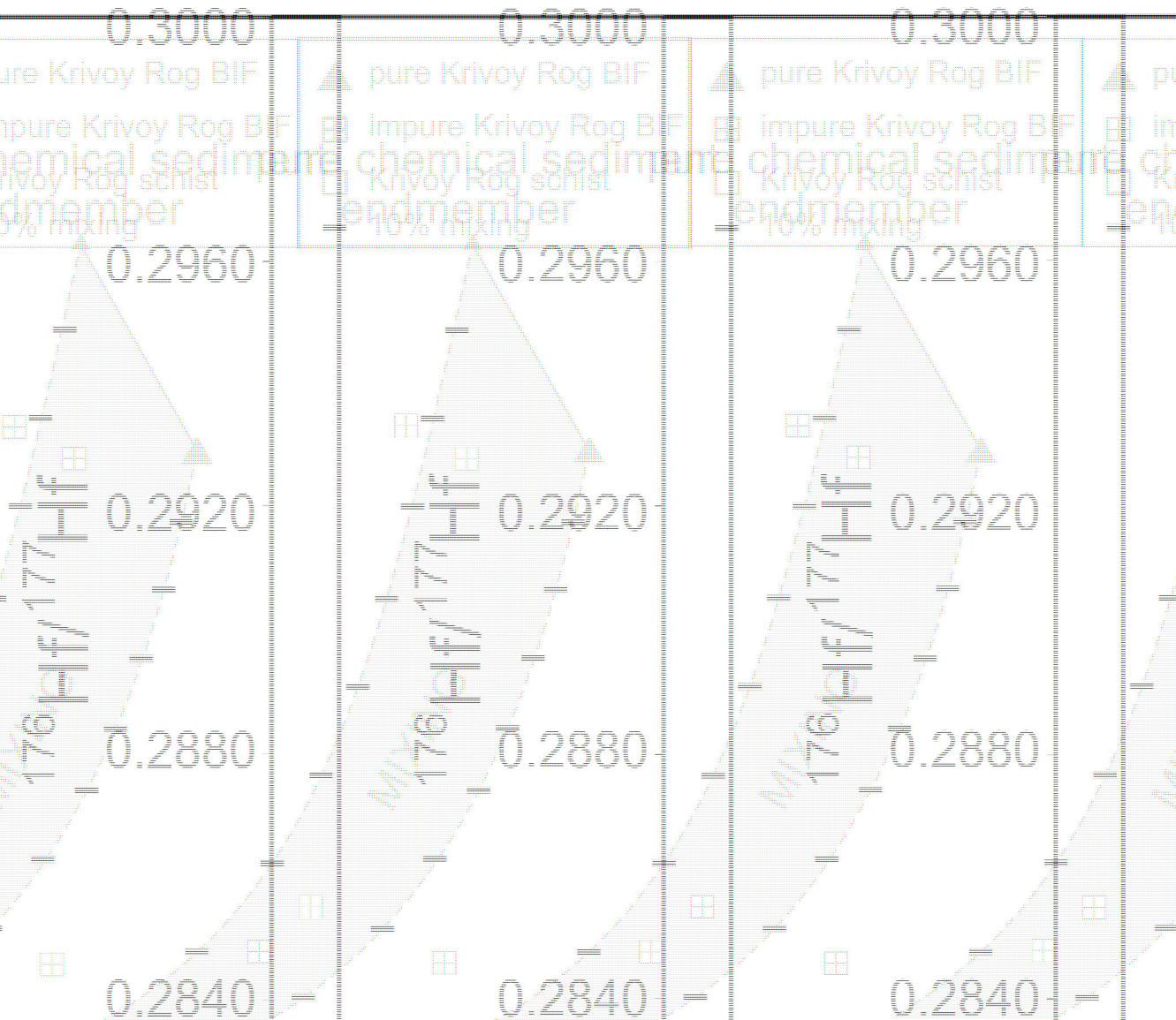
0.3000
0.2960
0.2920
0.2880
0.2840
pure Krivoy Rog BIF
impure Krivoy Rog BIF
chemical sediments
Krivoy Rog schist
endmember
mixing

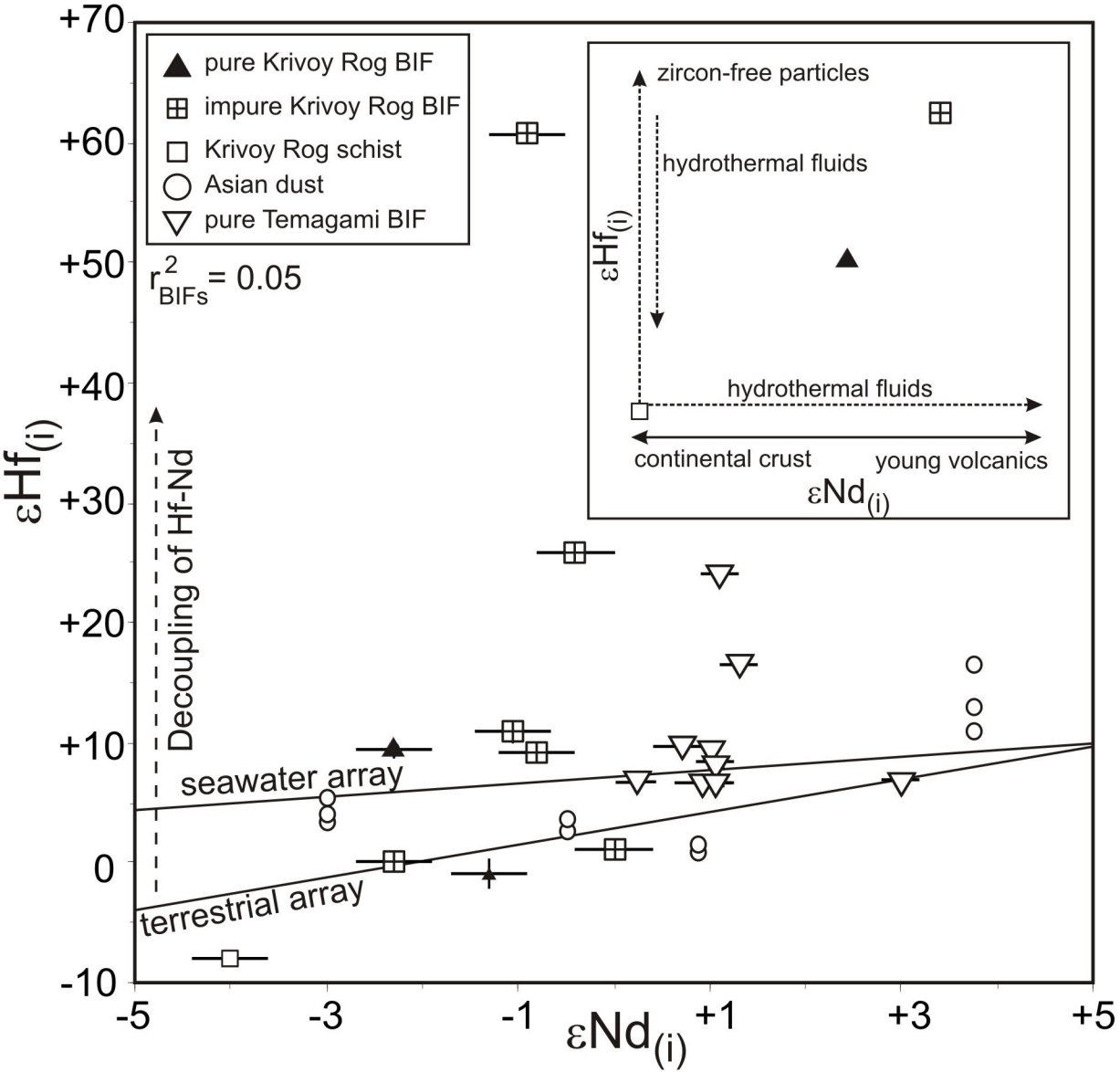
pure Krivoy Rog BIF
impure Krivoy Rog BIF
Krivoy Rog schist
Asian dust
pure Temagami BIF
r^2_{BIFs} = 0.05
zircon-free particles
hydrothermal fluids
$\varepsilon Hf_{(i)}$
hydrothermal fluids
continental crust
young volcanics
$\varepsilon Nd_{(i)}$
Decoupling of Hf-Nd
seawater array
terrestrial array
+70
+60
+50
+40
+30
+20
+10
0
-10
-5
-3
-1
+1
+3
+5

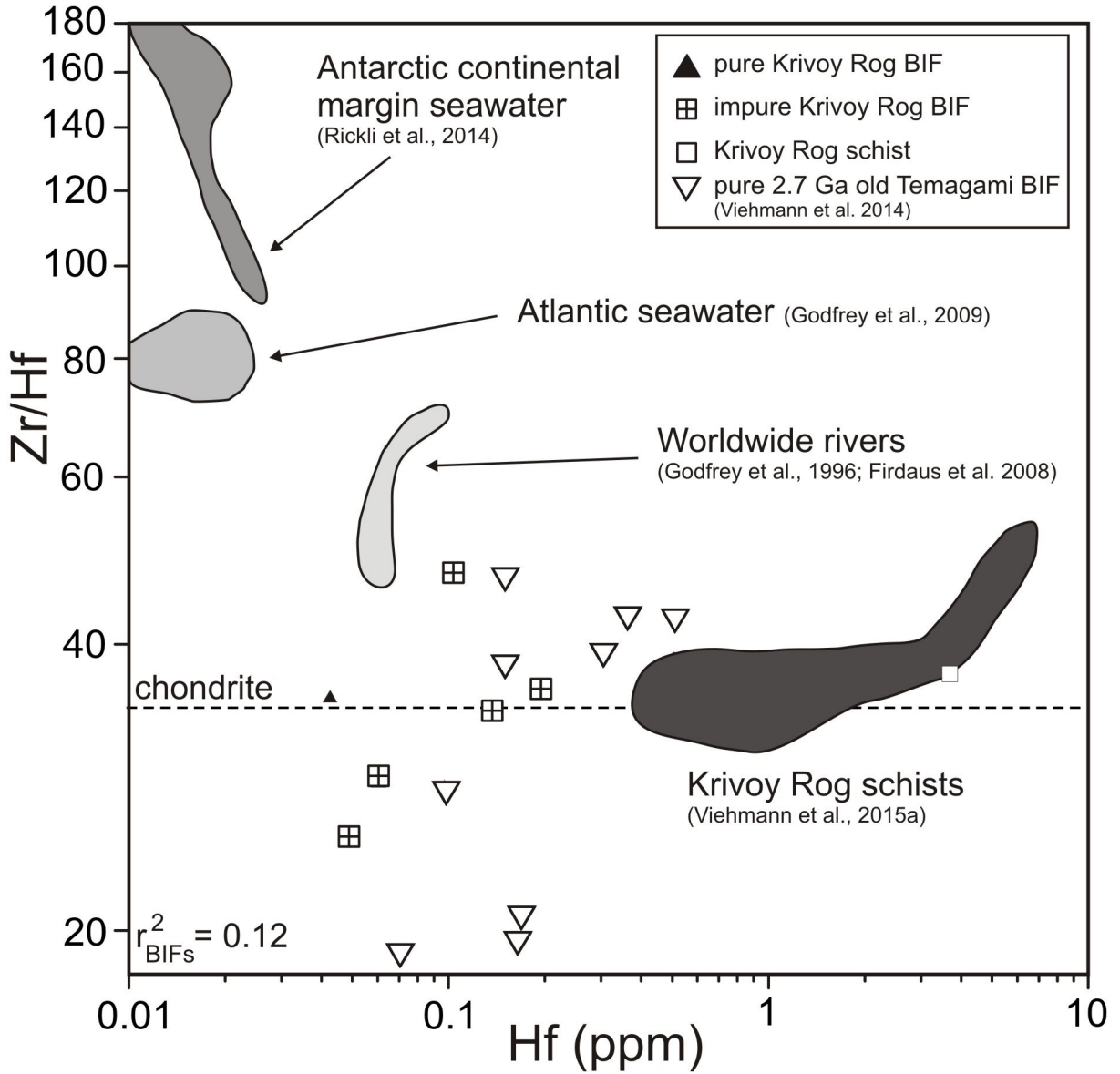
Antarctic continental margin seawater
(Rickli et al., 2014)
pure Krivoy Rog BIF
impure Krivoy Rog BIF
Krivoy Rog schist
pure 2.7 Ga old Temagami BIF
(Viehmann et al. 2014)
Atlantic seawater (Godfrey et al., 2009)
Worldwide rivers
(Godfrey et al., 1996; Firdaus et al. 2008)
chondrite
Krivoy Rog schists
(Viehmann et al., 2015a)
r^2_{BIFs} = 0.12
Zr/Hf
Hf (ppm)
180
160
140
120
100
80
60
40
20
0.01
0.1
1
10

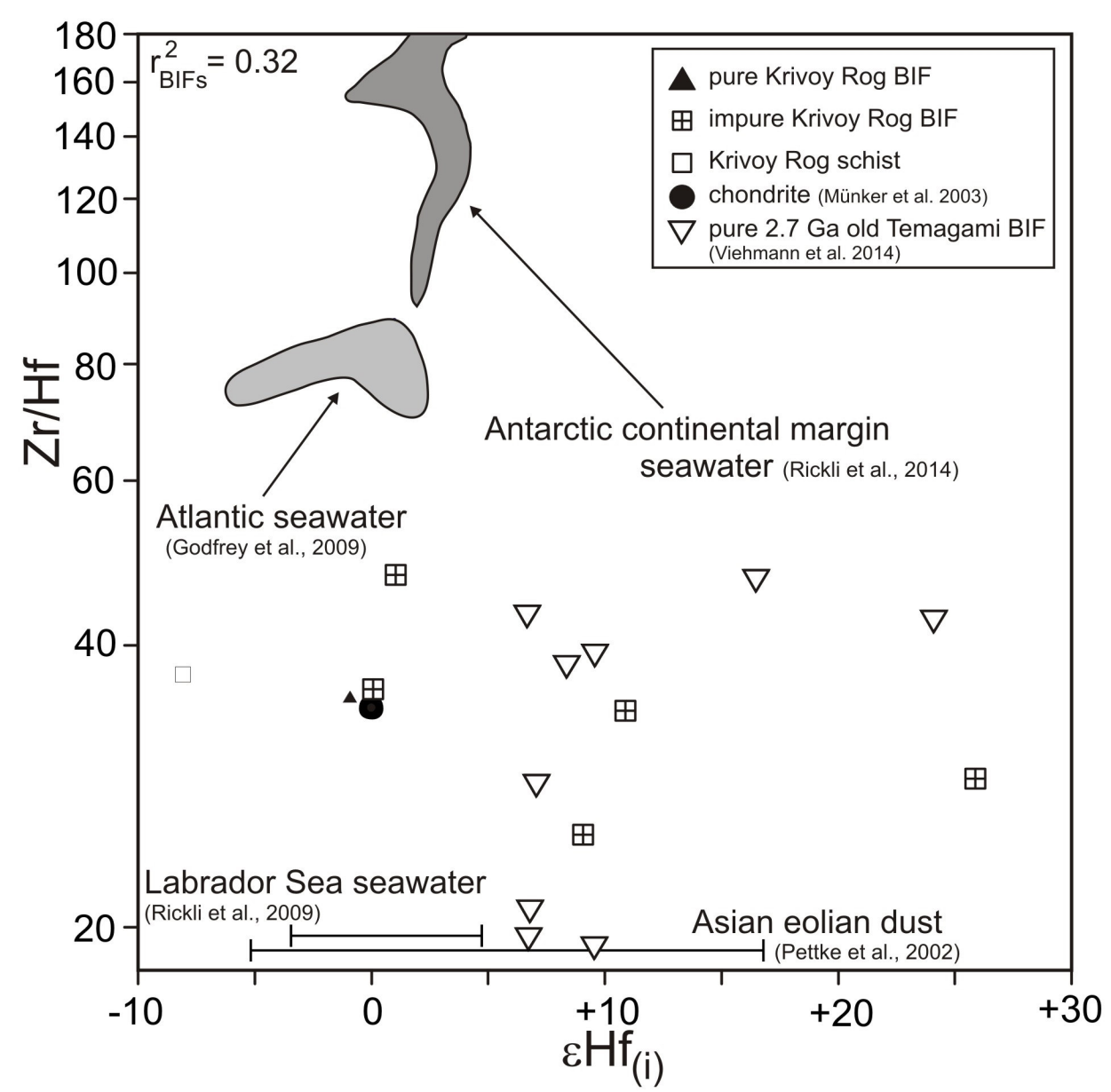
r^2_{BIFs} = 0.32
pure Krivoy Rog BIF
impure Krivoy Rog BIF
Krivoy Rog schist
chondrite (Münker et al. 2003)
pure 2.7 Ga old Temagami BIF (Viehmann et al. 2014)
Antarctic continental margin seawater (Rickli et al., 2014)
Atlantic seawater (Godfrey et al., 2009)
Labrador Sea seawater (Rickli et al., 2009)
Asian eolian dust (Pettke et al., 2002)
Zr/Hf
$\varepsilon Hf_{(i)}$
180
160
140
120
100
80
60
40
20
-10
0
+10
+20
+30

TABLE 1. Lu-Hf AND Sm-Nd ISOTOPIC COMPOSITIONS OF THE ~2.6 Ga KRIVOY ROG BIF

Sample	Material	Type	Sm [ppm]	Nd [ppm]	Lu [ppm]	Hf [ppm]	$^{147}Sm/^{144}Nd$	$^{143}Nd/^{144}Nd$	Zr/Hf	$^{176}Lu/^{177}Hf$	$^{176}Hf/^{177}Hf$	εHf(2.6)	εNd(2.6)
FUM 57	Fe-band	pure	0.143	0.634	0.0354	0.0218	0.1367	0.511497 ±6	-	0.23046	0.292844 ± 21	+9.48 ± 1.1	-2.3 ± 0.4
FUM 54	Fe-band	almost pure	0.609	2.96	0.0916	0.0425	0.1244	0.511337 ±6	35.3	0.30650	0.296334 ± 17	-0.91 ± 1.2	-1.3 ± 0.4
FUM 53	Fe-band	impure	0.302	1.67	0.0621	0.101	0.1096	0.511149 ±9	47.6	0.08695	0.285469 ± 19	+1.04 ± 0.7	+0.0 ± 0.4
FUM 55	Fe-band	impure	0.739	3.75	0.0654	0.137	0.1190	0.511229 ±6	34.1	0.06757	0.284780 ± 11	+10.9 ± 0.5	-1.6 ± 0.4
FUM 56	Fe-band	impure	0.581	2.81	0.0982	0.0604	0.1251	0.511396 ±8	28.8	0.23125	0.293344 ± 09	+25.9 ± 0.9	-0.4 ± 0.4
FUM 58	chert	impure	0.397	1.98	0.0443	0.195	0.1209	0.511226 ±9	35.9	0.03234	0.282725 ± 08	+0.08 ± 0.3	-2.3 ± 0.4
FUM 59	chert	impure	0.159	0.968	0.0222	0.0490	0.09938	0.510933 ±7	25.1	0.06427	0.2845667 ±14	+9.08 ± 0.5	-0.8 ± 0.4
FUM 60	chert	impure	0.318	1.41	0.0601	0.0427	0.1359	0.511553 ±8	-	0.20030	0.292782 ± 20	+60.6 ± 1.0	-0.9 ± 0.4
FUM 61	schist		4.35	28.3	0.524	3.70	0.09290	0.510659 ±7	37.3	0.02007	0.281886 ± 13	-8.06 ± 0.5	-4.0 ± 0.4

Note: Lu- Hf data are obtained by isotope dilution and MC-ICPMS, Zr and Nd isotope data are from Viehmann et al. (2015a). Errors are 2σ.